AFRL-RY-WP-TP-2013-0028

GAIN COUPLING VECSELs (POSTPRINT)

Robert Bedford

Optoelectronic Technology Branch
Aerospace Components & Subsystems Division

Chris Hessenius, Jerome Moloney, and Mahmoud Fallahi

Univerity of Arizona

Nathan Terry

United States Air Force Academy

JANUARY 2013
Interim

Approved for public release; distribution unlimited.

See additional restrictions described on inside pages

©2011 SPIE

STINFO COPY

AIR FORCE RESEARCH LABORATORY
SENSORS DIRECTORATE
WRIGHT-PATTERSON AIR FORCE BASE, OH 45433-7304
AIR FORCE MATERIEL COMMAND
UNITED STATES AIR FORCE

REPORT DOCUMENTATION PAGE

Form Approved
OMB No. 0704-0188

The public reporting burden for this collection of information is estimated to average 1 hour per response, including the time for reviewing instructions, searching existing data sources, gathering and maintaining the data needed, and completing and reviewing the collection of information. Send comments regarding this burden estimate or any other aspect of this collection of information, including suggestions for reducing this burden, to Department of Defense, Washington Headquarters Services, Directorate for Information Operations and Reports (0704-0188), 1215 Jefferson Davis Highway, Suite 1204, Arlington, VA 22202-4302. Respondents should be aware that notwithstanding any other provision of law, no person shall be subject to any penalty for failing to comply with a collection of information if it does not display a currently valid OMB control number. **PLEASE DO NOT RETURN YOUR FORM TO THE ABOVE ADDRESS**.

1. REPORT DATE *(DD-MM-YY)*	2. REPORT TYPE	3. DATES COVERED *(From - To)*
January 2013	Technical Paper	1 October 2009 – 11 January 2011

4. TITLE AND SUBTITLE
GAIN COUPLING VECSELs (POSTPRINT)

5a. CONTRACT NUMBER
In-house

5b. GRANT NUMBER

5c. PROGRAM ELEMENT NUMBER
62204F

6. AUTHOR(S)
Robert Bedford (AFRL/RYDH)
Chris Hessenius, Jerome Moloney, and Mahmoud Fallahi (University of Arizona)
Nathan Terry (United States Air Force Academy)

5d. PROJECT NUMBER
2002

5e. TASK NUMBER
IH

5f. WORK UNIT NUMBER
Y053

7. PERFORMING ORGANIZATION NAME(S) AND ADDRESS(ES)
Optoelectronic Technology Branch
Aerospace Components & Subsystems Division
Air Force Research Laboratory, Sensors Directorate
Wright-Patterson Air Force Base, OH 45433-7320
Air Force Materiel Command, United States Air Force

University of Arizona
United States Air Force Academy

8. PERFORMING ORGANIZATION REPORT NUMBER
AFRL-RY-WP-TP-2013-0028

9. SPONSORING/MONITORING AGENCY NAME(S) AND ADDRESS(ES)
Air Force Research Laboratory
Sensors Directorate
Wright-Patterson Air Force Base, OH 45433-7320
Air Force Materiel Command
United States Air Force

Air Force Office of Scientific Research AFOSR
875 North Randolph Street, Suite 325, Room 3112
Arlington, VA 22203-1768

10. SPONSORING/MONITORING AGENCY ACRONYM(S)
AFRL/RYDH

11. SPONSORING/MONITORING AGENCY REPORT NUMBER(S)
AFRL-RY-WP-TP-2013-0028

12. DISTRIBUTION/AVAILABILITY STATEMENT
Approved for public release; distribution unlimited.

13. SUPPLEMENTARY NOTES
Journal article published in Proc. SPIE 7945, 794508-1-9, 2011. ©2011 SPIE. The U.S. Government is joint author of the work and has the right to use, modify, reproduce, release, perform, display or disclose the work. PAO Case Number 88ABW-2012-6713, Clearance Date 28 December 2012. Report contains color.

14. ABSTRACT
Vertical external cavity surface emitting lasers (VECSELs) provide a flexible platform in order to explore curious laser designs and systems as their high-power, high-brightness make them attractive for many applications, and their flexibility eases this exploration. In considering the methods of coupling VECSELs as well as their potential uses, we begin by reporting on the development of a gain coupled VECSEL for use in optical switching. In particular, two VECSEL cavities share a common gain region; the competition for a common set of carriers dictate how these cavities interact. The easiest manifestation to realize gain coupling is to utilize a linear cavity as well as a v-cavity, built around a single half-VCSEL chip. The cavity gain/loss of each cavity can be controlled independently through use of birefringent filters, allowing us to explore the design space, which can be divided up into coarse behavior, easy to analyze through comparing the two uncoupled lasers, and a fine behavior, where one cavity will affect the other and each cavity can laser simultaneously, sometimes at dramatically different wavelengths. These two regions may be explained with simple rate equations, and it will be shown that if prepared properly, spontaneous emission plays a large role in balancing out the two laser cavities within the fine regime, while may be completely neglected in the coarse regime.

15. SUBJECT TERMS
Semiconductor, lasers

16. SECURITY CLASSIFICATION OF:			17. LIMITATION OF ABSTRACT:	18. NUMBER OF PAGES	19a. NAME OF RESPONSIBLE PERSON (Monitor)
a. REPORT	b. ABSTRACT	c. THIS PAGE			Robert Bedford
Unclassified	Unclassified	Unclassified	SAR	12	19b. TELEPHONE NUMBER *(Include Area Code)* N/A

Gain coupling VECSELs

Robert G. Bedford[a], Chris Hessenius[c], Nathan Terry[b], Jerome Moloney[c], and Mahmoud Fallahi[c]

[a]Air Force Research Laboratory, Wright-Patterson Air Force Base, Ohio
[b]Department of Physics, United States Air Force Academy, Colorado
[c]College of Optical Sciences, University of Arizona, Tucson, Arizona

ABSTRACT

Vertical external cavity surface emitting lasers (VECSELs) provide a laser design platform in order to explore a variety of systems, and their flexibility eases this exploration. Moreover, their high-brightness operation makes them attractive for many applications. In considering the methods of coupling VECSELs as well as their potential uses, we begin by reporting on the development of a gain coupled VECSEL for use in optical switching. In particular, two VECSEL cavities share a common gain region; the competition for a common set of carriers dictate how these cavities interact. The easiest manifestation to realize gain coupling is to utilize a linear cavity as well as a v-cavity, built around a single half-vertical cavity surface-emitting laser (VCSEL) chip. The cavity gain/loss of each cavity can be controlled independently through use of birefringent filters, allowing us to explore the design space, which can be divided up into coarse behavior, easy to analyze through comparing the two uncoupled lasers, and a fine behavior, where one cavity will affect the other and each cavity can lase simultaneously, sometimes at dramatically different wavelengths. These two regions may be explained with simple rate equations, and it will be shown that if prepared properly, spontaneous emission plays a large role in balancing the two laser cavities within the fine regime, while may be completely neglected in the coarse regime.

1. INTRODUCTION

Many of today's applications require high-brightness light sources in order to improve power consumption, obtain longer range and higher spatial resolution for remote sensing. Smaller, more environmentally robust sources are required for laser radar applications to maintain portability and/or be able to handle adverse environments (aircrafts, for example). The high gains readily achieved by semiconductor materials make them an attractive

The ability to integrate additional functionality to existing laser technology provides a potential advantage because such a laser platform may satisfy multiple applications, or be utilized durring "off-times" in another capacity. High brightness semiconductor lasers with wavelength switching capability are of great interest in a range of applications including free-space wavelength-multiplexed optical communication. Optically-pumped vertical external cavity surface emitting lasers (VECSEL) have proven to be very reliable in achieving multi-watt high brightness emission in a linear or v-cavity configuration.[1–3] The insertion of a birefringent filter in a VECSEL cavity allows narrow linewidth, widely tunable emission.[2,4] The "open-cavity" nature of the VECSEL also allows additional non-linear elements to be incorporated, such as semiconductor saturable absorber mirrors (SESAMs),[5] or nonlinear crystals for wavelength conversion.[6] In this paper we report for the first time gain coupling, switching, and dual wavelength operation in VECSELs by combining a linear-cavity and a v-cavity VECSEL sharing the same gain region. We present unique behaviors such as high-power optical switching and tunable dual-wavelength emission. Experimental results and supporting modeling results are reported.

This manuscript is laid out in the following manner. We first introduce a generic understanding of an arbitrary system of VECSELs in Section 2, wherein it is possible to couple multiple optical cavities and multiple chips, all operating in concert. Section 3 addresses the most basic component of the generic system: two optical cavities sharing a single gain, with only gain (and not photons) coupling the two cavities. We analyze specific regimes of this system operation. We first identify the "coarse" regime in Section 3.1 where the operation may be adequately predicted through analysis of the uncoupled laser cavities, and where we can change the system

Further author information (RGB): e-mail: robert.bedford@wpafb.af.mil

Vertical External Cavity Surface Emitting Lasers (VECSELs), edited by Ursula Keller, Proc. of SPIE
Vol. 7919, 791906 · © 2011 SPIE · CCC code: 0277-786X/11/$18 · doi: 10.1117/12.873864

Downloaded from SPIE Digital Library on 17 Jun 2011 to 134.131.125.50. Terms of Use: http://spiedl.org/terms

Approved for public release; distribution unlimited.

such that one of the cavities lases, and the other maintains zero output. We follow this with slightly more rigor in Section 3.2, identifying a unique behavior near where the two cavities have similar thresholds, which allows simultaneous lasing utilizing the same gain medium, even at vastly different wavelengths. In Section 3.3 we explore how the cavity lasing switching occurs, and theoretically, how we may modify and control the switching dynamics. Finally, we summarize our conclusions concerning this first step in VECSEL system dynamics in Section 4.

2. GENERIC VECSEL SYSTEMS

Due to the aforementioned open nature of the VECSEL system, it is possible to combine gain chips in much the same way one may add a nonlinear wavelength conversion filter or a SESAM. More peculiarly, it is possible to combine multiple laser cavities, only coupled through the gain material. In principal, we may expand the laser cavity to a system of optical cavities and gain elements, which may naturally lead to new behavior. In the "slow" regime (time-scales much longer than the photon lifetime), we chose to ignore all terms relative to N_b and arrive at a generalize I gain-element, J cavity set of coupled ordinary differential equations:

$$\frac{d}{dt}N_i = \frac{\Omega_w}{(\hbar\omega_p V_w)}P_i - \frac{N_i}{\tau_i} - v_g g_i \sum_{j=1}^{J} \frac{\Gamma_i^{(j)}}{\tilde{\Gamma}_i^{(j)}} S^{(j)} \tag{1}$$

$$\frac{d}{dt}S^{(j)} = -\frac{S^{(j)}}{\tau_p^{(j)}} + v_g S^{(j)} \sum_{i=1}^{I} \Gamma_i^{(j)} g_i \tag{2}$$

In these equations, N_i is the carrier density in chip i, and $S^{(j)}$ is the photon density in optical cavity j. $\Omega_w/(\hbar\omega_p V_w)$ is the number of carriers produced per unit power, and we have assumed this is the same for all chips. The carrier lifetime of the ith chip is given by τ_i*, while the photon lifetime is $\tau_p^{(j)}$ for the jth cavity in the system. The gain for each chip is g_i, the group velocity is v_g. The mode/gain overlap of cavity j with gain chip i is given by $\Gamma_i^{(j)}$. Finally, the ratio of overlaps in Equation 1 accounts for chips that may see multiple passes in a cavity as well as the contribution of each chip's RPG enhancement.

In this case, we can imagine one VECSEL cavity being the nonlinear element within another VECSEL cavity, and the nonlinearities between these two can potentially provide a rich capability that, as yet, remains predominantly unexplored.

3. GAIN-COUPLING CAVITIES: 2 CAVITIES, 1 GAIN

Equations 1 and 2 lend themselves to exceedingly complicated systems, and it becomes advantageous to understand the building blocks of the VECSEL system. The simplest case, containing a single chip and two cavities, is pictured schematically in Figure 1a. In this case, Equations 1 and 2 become a set of three coupled equations:

$$\frac{d}{dt}N = \widetilde{P} - \frac{N}{\tau} - \widetilde{g}\left(\Gamma_{r1}S^{(1)} + 2\Gamma_{r2}S^{(2)}\right) \tag{3}$$

$$\frac{d}{dt}S^{(1)} = -\frac{S^{(1)}}{\tau_p^{(1)}} + \widetilde{g}\Gamma^{(1)}S^{(1)} \tag{4}$$

$$\frac{d}{dt}S^{(2)} = -\frac{S^{(2)}}{\tau_p^{(2)}} + \widetilde{g}\Gamma^{(2)}S^{(2)}. \tag{5}$$

We have introduced $\widetilde{P}$ and $\widetilde{g}$, to simplify notation, equivalent to $\Omega_w/\hbar\omega_p V_w$ and v_g, respectively, In the scenario described by Equations 3-5, there are only three regimes that one may find themselves:

*Typically, carrier lifetime is separated into the constituent effects of non-radiative, spontaneous, and Auger effects, where $\tau_i^{-1} \equiv A_i + B_i N_i + C_i N_i^2$

Downloaded from SPIE Digital Library on 17 Jun 2011 to 134.131.125.50. Terms of Use: http://spiedl.org/terms

Approved for public release; distribution unlimited.

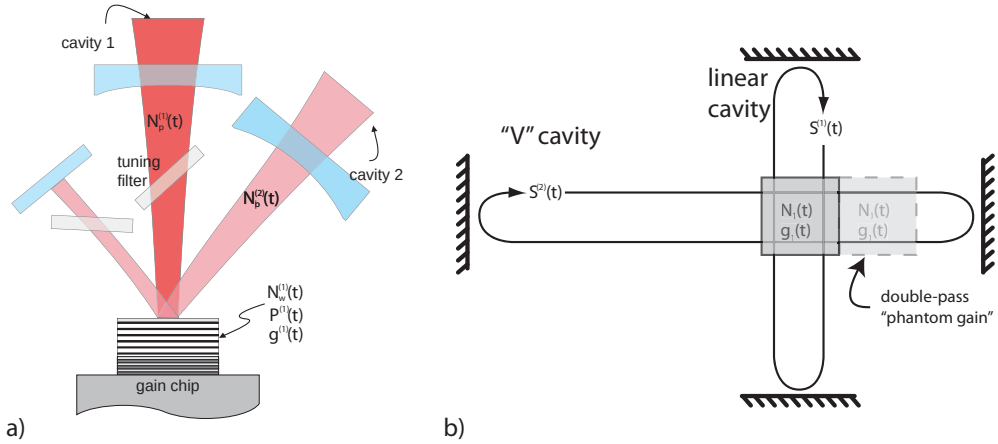

Figure 1. a) Physical set-up of two-cavity system, showing two cavity filters. b) Canonical schematic of coupled lasers.

Below threshold: $\widetilde{g} < \left(\Gamma^{(1)}\tau_p^{(1)}\right)^{-1}$ and $\widetilde{g} < \left(\Gamma^{(2)}\tau_p^{(2)}\right)^{-1}$ represent a particularly uninteresting regime. Both $S^{(1)}$ and $S^{(2)}$ tend toward zero.

Cavity 1 above threshold: If $\left(\Gamma^{(1)}\tau_p^{(1)}\right)^{-1} < \left(\Gamma^{(2)}\tau_p^{(2)}\right)^{-1}$, then at the point the material gain reaches the loss of cavity 1, it clamps such that $\widetilde{g} = \left(\Gamma^{(1)}\tau_p^{(1)}\right)^{-1}$. At pump powers above this point the $S^{(1)}$ increases monotonically, and $S^{(2)}$ remains zero.

Cavity 2 above threshold: If $\left(\Gamma^{(1)}\tau_p^{(1)}\right)^{-1} > \left(\Gamma^{(2)}\tau_p^{(2)}\right)^{-1}$, then at the point the material gain reaches the loss of cavity 2, it clamps such that $\widetilde{g} = \left(\Gamma^{(2)}\tau_p^{(2)}\right)^{-1}$. At pump powers above this point the $S^{(2)}$ increases monotonically, and $S^{(1)}$ remains zero.

Figure 1a shows how we can couple the lasers in such a way that Equations 3-5 adequately describe the system. In particular, linear cavities or v-cavities have been built around semiconductor gain for years. In the linear cavity ("cavity 1" in this case) places the semiconductor at one of two cavity mirrors. In this case, the mode passes through the gain twice in one round trip. However, in the v-cavity (labeled "cavity 2"), the gain chip acts as a fold in the cavity, composed of two external mirrors. In this case, the light propagates through the gain four times in a single round trip, accounting for the factor of 2 in front of the stimulated emission term in Equation 3. In a canonical depiction of this process, Figure 1b shows how each of these cavities interact with the gain. The "phantom gain" is depicted as a second piece of gain in the v-cavity, with the same carrier density and gain as the primary gain. The modal gain overlap between the two cavities is also different. The mode overlap Γ is typically given as the product of multiple overlaps:

$$\Gamma \equiv \Gamma_z \Gamma_T \Gamma_p \Gamma_R,$$

where Γ_z is the temporal longitudinal overlap of the geometric cavity with the active region (semiconductor between the DBR and air), Γ_p is the fraction of the quantum well within the active region, Γ_R is the RPG enhancement term,[7] and finally Γ_T is the mode overlap with the pumping region. The $\Gamma_z\Gamma_p$ product is then the temporal longitudinal overlap of the quantum wells with the geometric cavity.

With this understanding, for a particular cavity where the overlaps and lifetimes are fixed, only two of of the above cases will take place: either the system will be below threshold, or exclusively cavity 1 or cavity 2 will lase,

Downloaded from SPIE Digital Library on 17 Jun 2011 to 134.131.125.50. Terms of Use: http://spiedl.org/terms

Approved for public release; distribution unlimited.

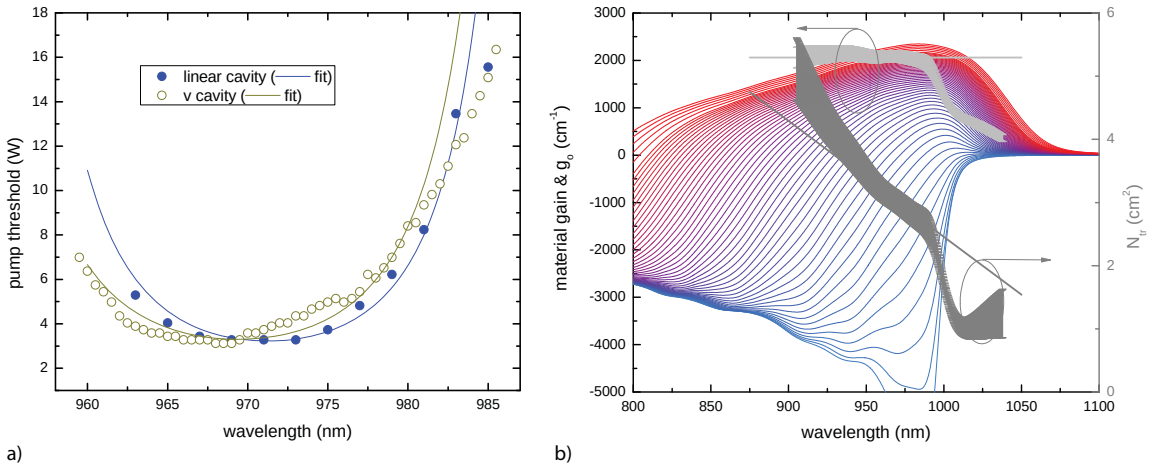

Figure 2. a) Experimental threshold of uncoupled lasers for different birefringent filter wavelength settings. b) Computed spectral gain curves, and numerically fit gain/carrier relation parameters. Error-bars give the standard deviation of the logarithmic fit to the actual computed relation.

depending on which cavity has a lower loss overlap ratio. To present more interesting possibilities, and direct control over the system, it is possible to include a birefringent filter into each cavity, and tune the cavity overlap of each cavity independently, changing both the gain and the overlap integral of each cavity independently.

The VECSEL gain chip used in the experiment is designed for emission around 975 nm. The active region consists of 14 InGaAs compressive strained quantum wells 8 nm thick surrounded by GaAsP strain compensation layers and AlGaAs pump-absorbing barriers. A 99.9% DBR stack made of 25 pairs of $Al_{0.2}Ga_{0.8}As/AlAs$ is grown on the top of the active region and a single layer quarter-wave low-reflection coating of SiO_2 is applied to the surface of the chip to enhance the 975 nm signal.

Cavity 1 consists of a single output coupler (OC) and birefringent filter positioned at Brewsters angle with a cavity length of 16 cm and a 350 μm mode size diameter on the VECSEL chip. Cavity 2 is folded at the VECSEL chip and has a highly reflective (HR) flat mirror at one end and a 96% reflective, 30 cm radius of curvature OC at the other end. The 3 cm separation between the HR flat mirror and the chip and 25 cm between the chip and the OC results in a mode diameter of $\sim$360 μm, which is similar to that of cavity 1. Cavity 1 has a natural photon lifetime of ($\tau_p^{(1)}$) of 18.75 ns, while in cavity 2, $\tau_p^{(2)}$=9.27 ns.

3.1 Coarse Tuning Characteristics

Utilizing the birefringent filters, it is possible to change the uncoupled threshold of the two separate cavities. This data is depicted in Figure 2a. In order to best understand the functional dependance of the threshold with wavelength, we can first predict the wavelength nature of the geometric cavity response. Reference 7 derives the relative confinement factor that results in a $1 + sinc$ function for normal incidence, whos argument is $\pi 2t/\lambda$ on resonance, where t is an individual quantum well thickness. In resonance Γ_r can approach 2. As we tune off resonance, it falls of as $\sim sinc$.

The other main wavelength-dependent term is the gain, which we also allow to vary with wavelength. Figure 2b shows how the gain shifts at a constant temperature as a function of carrier density. In this case, we take a simple logarithmic gain approximation, and allow the transparent carrier density to vary as a function of wavelength. Explicitly, this is written as:

$$g(N;\lambda) = g_0 \ln\left[\frac{N}{N_{tr}(\lambda)}\right].$$

Downloaded from SPIE Digital Library on 17 Jun 2011 to 134.131.125.50. Terms of Use: http://spiedl.org/terms

Approved for public release; distribution unlimited.

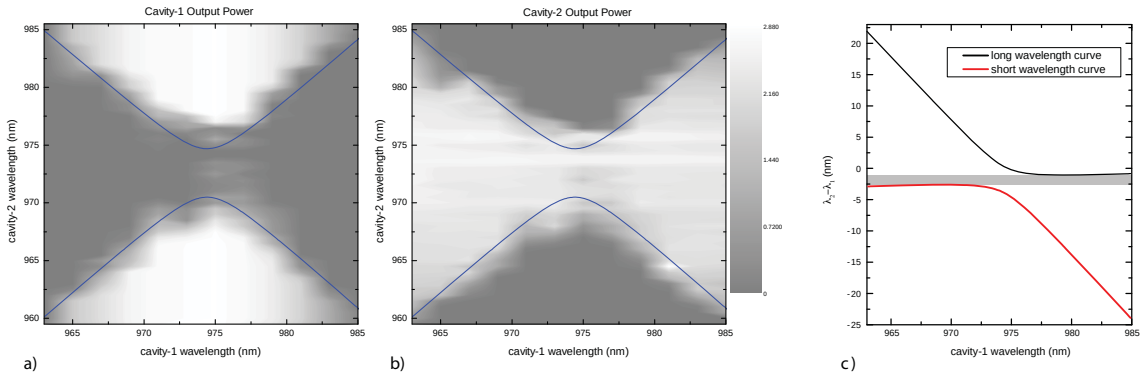

Figure 3. a) Experimental power out of cavity 1 as a function of the birefringent filter wavelength of each cavity. b) Experimental power out of cavity 2 as a function of the birefringent filter wavelength of each cavity. The uncoupled cavity boundaries are shown in blue in (a) and (b). c) The difference in operation wavelengths of each cavity near the equithreshold boundaries.

We maintain this approximation as suitable based on a gain calculation packaged SimuLase, using an 8×8 kp-model and including many-body Coulomb effects, and utilize this to fit our gain/carrier relation. Empirically, we determined the slope of the gain coefficient g_0 does not vary appreciably with wavelength, and all dependance is in the N_{tr} term. The transparency carrier density has nominally a linear dependance with wavelength over the fitted region of interest (∼950-980 nm).

Using the wavelength dependance in Γ_r and g, we can fit the experimental threshold data in Figure 2a to determine the slope of N_{tr} verses wavelength, as well as the RPG enhancement. We ignore thermal effects, our prediction at much larger pump powers should be suspect. We therefore chose to weigh the points near the lowest threshold the greatest, as this range has the most data all at somewhat the same power. Our fit to experimental data is depicted in Figure 2a by the lines. The majority of the curvature of this function is due to the variation of Γ_r with respect to wavelength. The gain/carrier relation's wavelength dependance offers comparatively little influence, although the asymmetry in Figure 2a is due solely to this effect.

Because we understand that when one laser threshold is below the other, that cavity lases, effectively clamping the gain at threshold and forbidding the other cavity to lase, we can utilize the birefringent filters in each cavity to select the the cavity loss (and therefore threshold). For a given pair of wavelength settings, we predict the coupled effect by referring to Figure 2a, determining which cavity is lasing, repeating this approach for every combination of filter settings.

Although tedious, it is possible to use the two filters to acquire data over two dimensions (one for each filter wavelength), taking data for each cavity output to confirm this scheme. The power of each cavity is plotted in these two birefringent filter wavelength settings in Figure 3a-b. We can immediately see the two regions identified by our original theoretical framework. Moreover, the region separating the two regions are identified over the boundary where $\Gamma^{(2)}\tau_p^{(2)} = \Gamma^{(1)}\tau_p^{(1)}$, where we can turn either of the lasers completely off. This boundary, identified numerically in blue in Figure 3 and 3b (from fits in Figure 2a) is unstable and not achievable in practice due to noises in real systems. However, the analysis utilizing uncoupled analysis to the coupled cavity power results show agreement is quite good.

This system also is interesting because is it possible to operate near the $\Gamma^{(2)}\tau_p^{(2)} = \Gamma^{(1)}\tau_p^{(1)}$ boundary for two cavity settings over a broad wavelength region. For example, in the upper left of Figure 3, λ_1 ∼963 nm, while λ_2 ∼985 nm. A switch from one to the other results in a lasing wavelength change of 22 nm with almost no change in the cavity. Likewise, in the lower right of Figure 3 represents a switch of almost 24 nm. Conversely, the diagonal from lower left to upper right represents wavelengths of each cavity that are almost identical to each other (∼ 2 nm switches). This boundary wavelength difference in cavity 1 and cavity 2 is plotted in Figure 3c.

Downloaded from SPIE Digital Library on 17 Jun 2011 to 134.131.125.50. Terms of Use: http://spiedl.org/terms

Approved for public release; distribution unlimited.

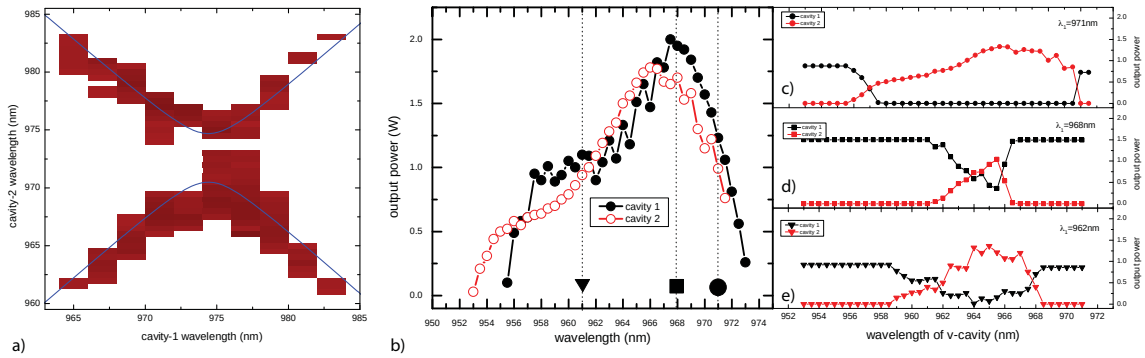

Figure 4. a) Region as in Figure 2, but just identifying region where two chips laser simultaneously. b) Output power of each uncoupled cavity as a function of birefringent tuning filter wavelength. c-e) Output power of each *coupled* cavity as a function of birefringent tuning filter for different birefringent filter settings.

3.2 Fine Tuning Characteristics

While in the previous section, we stated the boundary is unstable and not suitable to observe in experimental systems, we see in practice that both lasers can lase simultaneously. Figure 4a is a complimentary plot to Figure 3 where we identify the region in red where both cavities have non-zero outputs. Equations 3-5 do not predict this, leaving us to modify our theory to account for the effect.

We previously admit to arrive at Equations 3-5 through the use of numerous approximations, including neglecting the barrier carriers, thermal effects, incoherent terms, and the fast varying effects. To better explain the equithreshold region, we judiciously reintroduce spontaneous emission, primarily because of its effect near threshold, although the contribution well above threshold is typically negligible. Rewriting Equations 4-5 to include spontaneous emission gives:

$$\frac{d}{dt}S^{(1)} = -\frac{S^{(1)}}{\tau_p^{(1)}} + \widetilde{g}\Gamma^{(1)}S^{(1)} + \beta^{(1)}BN^2 \tag{6}$$

$$\frac{d}{dt}S^{(2)} = -\frac{S^{(2)}}{\tau_p^{(2)}} + \widetilde{g}\Gamma^{(2)}S^{(2)} + \beta^{(2)}BN^2, \tag{7}$$

where $\beta^{(j)}$ is the jth cavity mode cross-section with the spontaneous emission radiation, B is the spontaneous emission coefficient, a contribution to τ in Equation 3. Using this, we can redefine the boundary between the two modes as:

$$\frac{1}{\tau_p^{(1)}} - \widetilde{g}\Gamma^{(1)} = \frac{\beta^{(2)}S^{(2)}}{\beta^{(1)}S^{(1)}}\left(\frac{1}{\tau_p^{(2)}} - \widetilde{g}\Gamma^{(2)}\right), \tag{8}$$

and is no longer independent of photon density.

Figure 4b represents the uncoupled "tuning curves" (output power) as a function of the birefringent filter wavelength for each cavity. This is the most common data presented when discussing VECSEL tuning.[8,9] The three dotted lines in these tuning curves represent the settings for the filter in cavity 1 shown in Figures 4c-e. In these plots, the output in each cavity is shown as a function of the filter wavelength setting within cavity 2. These plots are the equivalent of single vertical traces of the two-dimensional plots shown in Figure 3, including the boundary regime in which both cavities have non-zero outputs. The width of the non-zero regime can be changed, depending on the relative change of the threshold as a function of wavelength. Because the slope does not change significantly as a function of wavelength, Figure 4b shows us that because the $\partial P/\partial\lambda$ is smaller on

Downloaded from SPIE Digital Library on 17 Jun 2011 to 134.131.125.50. Terms of Use: http://spiedl.org/terms

Approved for public release; distribution unlimited.

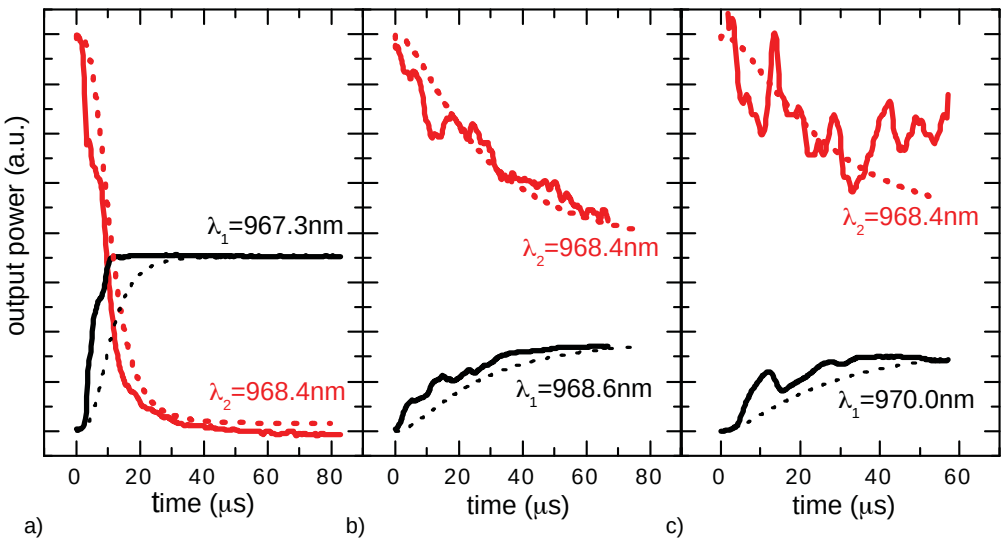

Figure 5. Plot of experimental output power versus time for different cavity tunings. The linear cavity was chopped in the dual cavity configuration. a) Cavity tuned such that cavity switches from completely on to completely off b)-c) various tuning such that the switching is less complete. Simulated results are shown as dotted lines.

the blue-side of the tuning peak than on the red side, the near-equithreshold region is expanded. There are also regions where we can tune completely through spectrum without turning off cavity 1. Two of these cases are shown in Figures 4d-e.

3.3 Dynamics

To observe the transient response of the optical switch between the two cavities, both in the coarse and fine tuning regimes, we utilize silicon detectors with a 3-dB frequency of 200 MHz to simultaneously detect output from each cavity. These are coupled to a 500 MHz oscilloscope. An optical chopper is placed within cavity 1, periodically blocking and unblocking lasing from occurring. Cavity 2 is tuned to a wavelength providing a higher threshold than cavity 1, such that when cavity 1 is blocked, cavity 2 builds up and switches "on". The chopper triggers the oscilloscope to acquire the build-up, not when cavity 1 is blocked, but rather when it is unblocked. We see three examples of this switching in Figure 5.

When spontaneous emission is included, the gain coupling can prevent one cavity running away and the other shutting off completely. Consider the case shown in Figures 5b and 5c where cavity 1 and cavity 2 are very near equithreshold spectral regions. Here we see cavity 1 is initially blocked and then unblocked at time t=0. The uncoupled threshold of cavity 1 is initially slightly lower and the photon density increases at the expense of the photon density of cavity 2. As the photon density of cavity 2 drops, the relative contribution of the spontaneous emission increases. Because spontaneous emission is an additive term to the photon equation, it can be considered as a mechanism for reducing the threshold gain of cavity 2, thus lowering the uncoupled threshold of cavity 2 below that of cavity 1 and effectively reducing the photon density of cavity 1. This cycle is damped by the photon lifetime allowing both cavities to operate simultaneously. This effective reduction in the threshold is of course, very small, which is why this effect is important only when the two uncoupled thresholds are very close.

The significant oscillations seen in Figure 5b-c are not seen in the numerical solution to Equation 3 and Equations 6-7, where the dotted-line numerical simulations shown in Figure 5. Near threshold, the relative cavity loss, caused by misalignments, for example, become extremely important. Small fluctuations caused by vibration and air currents can manifest in vast changes power out of the laser, selecting one cavity over the other.

Downloaded from SPIE Digital Library on 17 Jun 2011 to 134.131.125.50. Terms of Use: http://spiedl.org/terms

Approved for public release; distribution unlimited.

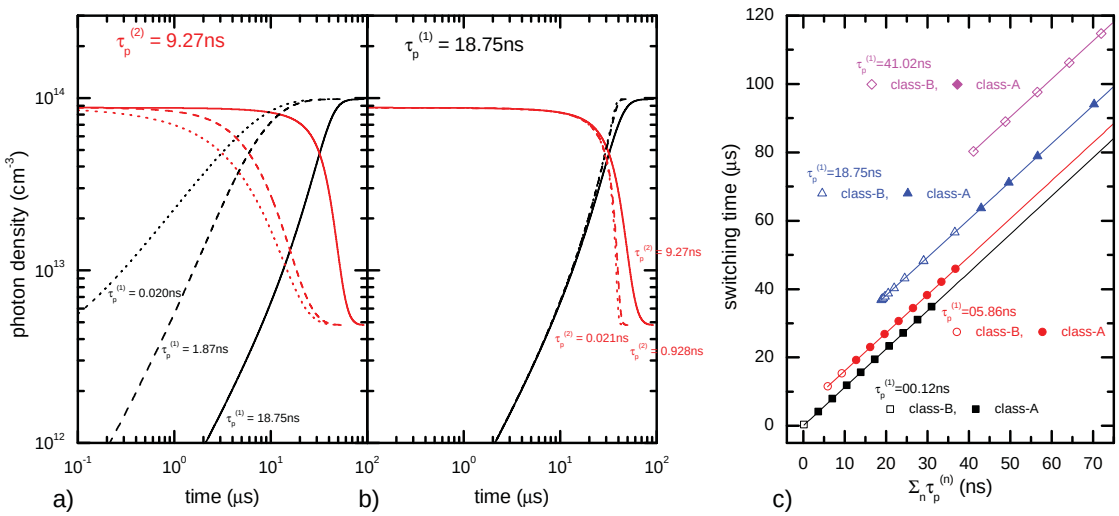

Figure 6. Photon dynamics for various combinations of photon lifetimes. a) Holding $\tau_p^{(2)}$ constant, and changing $\tau_p^{(1)}$ through the carrier lifetime. b) Holding $\tau_p^{(1)}$ constant while changing $\tau_p^{(2)}$ through various photon lifetimes. c) Cavity switching time as a function of net photon lifetime, holding $\tau_p^{(1)}$ constant at several values. This last plot shows that the linear relation holds, although there must be an effective offset for every value of $\tau_p^{(1)}$.

Experimentally, we take particular care to ensure there is no photon coupling directly from one cavity to the other, as this may cause laser instabilities, which could also cause such "noises". This direct coupling could be due to inadvertent semiconductor surface imperfection induced scattering. However, because birefringent filters are in each cavity, any photons scattered from one cavity to the other are immediately removed from the cavity provided the two filters are at different, non harmonic, wavelengths. We see the oscillation in Figure 5b-c for all settings of wavelengths along the boundary identified in Figure 4a.

To understand the limitations of such a switch as depicted in Figure 5, we look at the case of a "pure" class-A laser. In this system, the turn-on time is derived as:

$$T_b = \frac{\tau_p}{r-1} \ln\left(\frac{I_{ss}}{I_\circ}\right), \tag{9}$$

where τ_p is the photon lifetime, r is the normalized ratio of round trip gain to loss, (presumed to be greater than unity), and I_{ss} and $I_\circ$ is the saturation power density and initial noise power density, respectively.[10] This derivation is predicated on the fact that the optical gain of the material remains high until the laser hits some saturation level, at which time the gain begins to drop quickly, and causes the power to cease increasing exponentially. While not strictly applicable in this case, Equation 9 maintains qualitative agreement with experiments.

In a VECSEL switch, we build up from spontaneous emission, therefore $\ln(I_{ss}/I_\circ) \sim 17$. In near equithreshod regions, $(r-1) \sim 10^{-3}$, which results in a relatively slow coupled-cavity switch, significantly greater than 1 μs. We simulate the switching time by allowing the cavity to settle down with cavity 1 "blocked" (significantly increasing the cavity loss). Therefore cavity 2 is allowed to lase, reaching a steady-state value. At time t=0, we numerically "unblock" cavity 1 (returning its cavity loss to the normal value), which is slightly lower than that of cavity 1.

A typical computed "switch" can be see in Figure 6, where the cavities have very similar thresholds. Figure 6a shows a switch where cavity 2 starts out in a lasing mode, and cavity 1 begins at near zero (just spontaneous emission). When cavity 1 is unblocked (at time t=0), photons begin building up, depleting carriers and thus

Downloaded from SPIE Digital Library on 17 Jun 2011 to 134.131.125.50. Terms of Use: http://spiedl.org/terms

Approved for public release; distribution unlimited.

reducing cavity 2 photons. The particular simulated case does not turn off cavity 2 completely, so it is a scenario somewhat like that of Figure 5b or Figure 5c, and that found in.[11] The total photons increase slightly (because cavity 1 threshold is slightly lower than cavity 2).

We do many simulations like those seen in Figure 6a and 6b, allowing cavity 2 photon lifetime to vary while holding $\tau_p^{(1)}$ at constant values. $\tau_p^{(2)}$ is varied to traverse the class-B to class-A transition in a traditional uncoupled cavity (where uncoupled carrier lifetime is approximately 5 ns). We take the switching time to be $(1-e^{-2})S^{(2)}(t_{final})$, and numerically determine the time at which that occurs. This is plotted in Figure 6c as a function of total photon lifetime. We see that the switching time is linear with $\sum_n \tau_p^{(n)}$, consistent with a class-A laser approximation in Equation 9. Because the photons in cavity 1 mitigate the carrier response speed of the chip, we use cavity 1 photon lifetime as dominating the "effective carrier lifetime". This "effective carrier lifetime" is then used to determine class-A or class-B ($\tau_p^{(2)}/\tau_p^{(1)}$ >1 being class-A) in Figure 6.

The predictive nature of Equation 9 still adequately describes this system, even though the system is not strictly a class-A cavity. The slight offset to each curve in Figure 6c also shows us that we must add an effective additive lifetime of $\sim 0.75\tau_p^{(1)}$ to the photon lifetime in order to have the best agreement with Equation 9. In essence, the switching time goes as Equation 9 provided the effective photon lifetime is $1.75\tau_p^{(1)} + \tau_p^{(2)}$.

We expect in a class-A laser that the gain remains flat while the photons build-up until the saturation point, at which time they drop to the final value, much faster than the photon build-up time. However, when the carrier dynamics are on par with the photon dynamics, the gain changes more slowly throughout the switch. In the case of the gain-coupled VECSEL, the initially lasing cavity (in this case cavity 2) photon dynamics mitigate the carriers in cavity 1 directly. As cavity 2 photon lifetime is short, so is the effective carrier lifetime that cavity 1 experiences, and therefore the cavity in this case operates in an effective class-A regime. When the photon lifetime of cavity 2 is significantly larger than that of cavity 1, the effective carrier lifetime is greater than the photon lifetime in cavity 1, and the laser should operate in an effective class-B regime. For most VECSEL cavities, including the experimental case represented in Figure 5, this regime is very near the border of the two classes. We can then call this switching an effective change of laser classes.

Experiments are somewhat complicated by the fact that chip damage is routinely observed readily when both cavities are lasing simultaneously. Although a concrete understanding of this phenomena remains elusive, such damage may result from localized hot-spots in spatial regions where both cavities have coherent interference. Studies are ongoing as to the significance of this damage, and whether there is a suitable technique to circumvent this damage.

4. CONCLUSION

The dual cavity design allows for gain coupling of VECSEL laser cavities. We examined the simplest case that employs a linear cavity and v-cavity that are gain coupled. This coupling allows not only optical switching between two cavities operating at different wavelengths, but also the simultaneous generation of different wavelengths from a common gain medium, at wavelengths anywhere near the boundary where the two laser thresholds are similar; we experimentally demonstrate lasing at two simultaneous wavelengths up to 22 nm apart. A fundamental set of rate equations is used to define an operation map where the areas of simultaneous operation and switching regions are plotted.

We have numerically and experimentally identified and explained the boundary lines between linear and v-cavity dominance defining the tuning capabilities of the dual wavelength generation. In the regime where the two cavities have close thresholds, we show that spontaneous emission is critical to the explanation. We are able to reproduce the approximate shape of experimental shifts by fitting the wavelength-dependent cavity overlap as well as the wavelength-dependent gain/carrier relation. We show it is suitable to represent the switch as an "effective" class-A laser. This building-block component of the generic VECSEL system gives us insight into what may be possible in a larger system of VECSEL cavities. In addition, it may be possible to expand the system to include several cavities centered on a common gain medium to allow for even more flexibility.

Downloaded from SPIE Digital Library on 17 Jun 2011 to 134.131.125.50. Terms of Use: http://spiedl.org/terms

Approved for public release; distribution unlimited.

ACKNOWLEDGMENTS

This work was supported by AFOSR through lab task 08RY08COR. The authors would also like to acknowledge support from the State of Arizona TRIF Photonics Foundation.

REFERENCES

1. J. Chilla, S. Butterworth, A. Zeitschel, J. Charles, A. Caprara, M. Reed, and L. Spinelli, "High power optically pumped semiconductor lasers," in *Proc. SPIE - Int. Soc. Opt. Eng.*, 2003.
2. L. Fan, M. Fallahi, A. Zakharian, J. Hader, J. Moloney, R. Bedford, J. Murray, W. Stolz, and S. Koch, "Extended tunability in a two-chip vecsel," *IEEE Photon. Tech. Lett.* **19**, pp. 544–546, April 2007.
3. T.-L. Wang, Y. Kaneda, J. Yarborough, J. Hader, J. Moloney, A. Chernikov, S. Chatterjee, S. Koch, B. Kunert, and W. Stolz, "High-power optically pumped semiconductor laser at 1040 nm," *IEEE Photon. Tech. Lett.* **22**, pp. 661–663, May 2010.
4. J.-M. Hopkins, A. J. Maclean, D. Burns, E. Riis, N. Schulz, M. Rattunde, C. Manz, K. Köhler, and J. Wagner, "Tunable, single-frequency, diode-pumped 2.3μm vecsel," *Opt. Exp.* **15**(13), pp. 8212–8217, 2007.
5. R. Häring, R. Paschotta, A. Aschwanden, E. Gini, F. Morier-Genoud, and U. Keller, "High-power passively mode-locked semiconductor lasers," *IEEE J. of Quant. Elect.* **2**, pp. 1268–1275, Sept. 2002.
6. J. Chilla, H. Zhou, E. Weiss, A. Caprara, Q. Shou, S. Govorkov, M. Reed, and L. Spinelli, "Blue & green optically-pumped semiconductor lasers for displays," in *Proc. SPIE - Int. Soc. Opt. Eng.*, 2005.
7. S. Corzine, R. Geels, J. Scott, R. H. Yan, and L. Coldren, "Design of Fabry-Perot surface-emitting lasers with a periodic gain structure," *IEEE J. of Quant. Elect.* **25**(6), pp. 1513–1524, 1989.
8. L. Fan, M. Fallahi, J. T. Murray, R. Bedford, Y. Kaneda, A. R. Zakharian, J. Hader, J. V. Moloney, W. Stolz, and S. W. Koch, "Tunable high-power high-brightness linearly polarized vertical-external-cavity surface-emitting lasers," *App. Phy. Lett.* **88**(2), p. 021105, 2006.
9. J. Paajaste, S. Suomalainen, R. Koskinen, A. Hrknen, M. Guina, and M. Pessa, "High-power and broadly tunable GaSb-based optically pumped VECSELs emitting near 2 μm," *J. of Crys. Growth* **311**(7), pp. 1917–1919, 2009. International Conference on Molecular Beam Epitaxy (MBE-XV), The 15th International Conference on Molecular Beam Epitaxy (MBE-XV).
10. A. Siegman, *Lasers*, University Sciences Books, 1986.
11. C. Hessenius, N. Terry, M. Fallahi, J. Moloney, and R. Bedford, "Gain coupling of class a semiconductor lasers," *Opt. Lett.* **35**, pp. 3060–3062, Sep 2010.

Downloaded from SPIE Digital Library on 17 Jun 2011 to 134.131.125.50. Terms of Use: http://spiedl.org/terms

Approved for public release; distribution unlimited.